(Springer-Verlag, New York, 1984).
20. H. M. Berman, *Curr. Opin. Struct. Biol.* **4**, 345 (1994).
21. C. R. Calladine and H. R. Drew, *Understanding DNA, the Molecule and How It Works* (Academic Press, London, 1992).
22. N. Davidson and W. Szybalski, in *The Bacteriophage Lambda*, A. D. Hershey, Ed. (Cold Spring Harbor Laboratory, Cold Spring Harbor, NY, 1971), p. 56.
23. Betaine has been shown to lower the melting temperatures of CG base pairs to the same value as that of AT base pairs [W. A. Rees, T. D. Yager, J. Korte, P. H. von Hippel, *Biochemistry* **32**, 137 (1993)]. Interestingly, the effect of betaine may have been just the opposite, that is, to enhance the difference between the forces required to induce the transition in AT- and CG-rich regions.
24. The fitted Kuhn segment length of 15 Å implies a persistence length of 7.5 Å for ssDNA. This value is about half that estimated by E. K. Achter and G. Felsenfeld [*Biopolymers* **10**, 1625 (1971)] for apurinated ssDNA by using light scattering and sedimentation. It was assumed in that study that 1 M NaCl is a theta solvent for ssDNA. In the present study, the contractile force on a ssDNA molecule in 1 M NaCl, extrapolated to zero extension, was about 5 pN (see Fig. 6, inset blue). This force offset probably indicates secondary structure formation or condensation within the molecule. If such structure formed in the sedimentation studies, then an erroneously large value for the rigidity of ssDNA and for RNA could have been obtained.
25. In the presence of adenosine triphosphate (ATP) or ATP[γ]S, RecA undergoes an alosteric change into a high-affinity form that binds dsDNA cooperatively in a stoichiometric ratio of 1 RecA/3 bp of dsDNA to form a right-handed helical filament [S. C. West, *Annu. Rev. Biochem.* **61**, 603 (1992)]. There are six RecA molecules and 18.6 bp/turn of the DNA molecule that is overstretched by a factor of 1.5 times its B-form contour length.
26. A. Klug and F. H. C. Crick [*Nature* **255**, 530 (1975)] have suggested that formation of a few highly bent regions or "kinks" in DNA might be energetically favorable relative to smooth bending over a longer DNA length. The argument requires that after the ensuing of a localized kink in the DNA molecule, the energy required to bend the DNA further by an angle θ at that location, be smaller than the energy needed to bend the DNA by the same angle before the ensuing of the kink. This is indeed observed in macroscopic elastic media when the deformation goes beyond the elastic into the "plastic" regime (a plastic straw is a good example).
27. Carboxylate-polystyrene beads (3.54 μm in diameter, CV = 2.7%, Spherotech) were covalently coated with streptavidin using 1-ethyl-3-(3-dimethylaminopropyl) carbodiimide (EDAC). Each molecule was pulled both right and left from the pipette to determine the point of attachment of the molecule on the pipette bead. Because the optically trapped bead can rotate freely, but the pipette-trapped bead cannot, *Ex* can be determined in absolute units (micrometers). In each *F-Ex* curve, data representing the following four processes is superimposed: extending the molecule to right of the pipette, then relaxing it from the right, extending it leftward, then relaxing it from the left. Each data point was taken after a ~0.5 μm change in extension and a 2-s waiting period. The force signal was then averaged for an additional 2 s and recorded. A complete right-left stretch cycle took about 10 min.
28. A video showing actual bead-DNA-bead assembly (Fig. 1B) can be viewed on the World Wide Web at <http://alice.uoregon.edu/~mark/>.
29. D. W. Ussery, R. W. Hoepfner, R. R. Sinden, *Methods Enzymol.* **212**, 242 (1992).
30. J. E. Hearst, S. T. Isaacs, D. Kanne, H. Rapoport, K. Straub, *Q. Rev. Biophys.* **17**, 1 (1984).

31. We thank D. Stigter, E. Siggia, J. Marko, and A. Hausrath for many useful discussions. This work was supported by NSF grants MBC 90118482 and BIR 9318945, and by NIH grant GM-32543. Partial support was provided by the Lucille P. Markey Foundation.

15 December 1995; accepted 12 January 1996

On the Nature of Water Bound to a Solid Acid Catalyst

L. Smith, A. K. Cheetham,* R. E. Morris, L. Marchese, J. M. Thomas,* P. A. Wright, J. Chen

The nature of the species formed when water interacts with Brønsted acid sites in a microporous solid acid catalyst, HSAPO-34, was studied by powder neutron diffraction and infrared spectroscopy. Previous infrared and computational studies had failed to unambiguously establish whether water is protonated to form hydronium (H_3O^+) ions or is merely hydrogen-bonded to acid sites inside the zeolite. Our experiments clearly showed that both species are present: An H_3O^+ ion is found in the eight-ring channel of the zeolite and a second water molecule is hydrogen-bonded to an acid site on the six-ring.

To understand more about the nature of the acid sites on solid catalysts is of both fundamental and profoundly practical importance. A probe molecule of more than academic interest in ascertaining the strength of the Brønsted acidity (proton-donating power) is water. Although the donating propensity of a bridging hydroxyl in aluminosilicate and silicoaluminophosphate (SAPO) catalysts (Scheme I) is known to be high, the most sophisticated quantum mechanical computations reveal (*1*) that no hydronium ions (structure III, Scheme I) form, just hydrogen-bonded species (structure II, Scheme I). Although some experimental studies may be interpreted in these terms (*2*), others (*3*) point strongly to the formation of H_3O^+. Because solid (molecular sieve) catalysts are extensively used petrochemically (*4*) and are central in the design of superior materials for converting alkanes to branched-chain isomers of higher octane number, it is important to elucidate their Brønsted acidity.

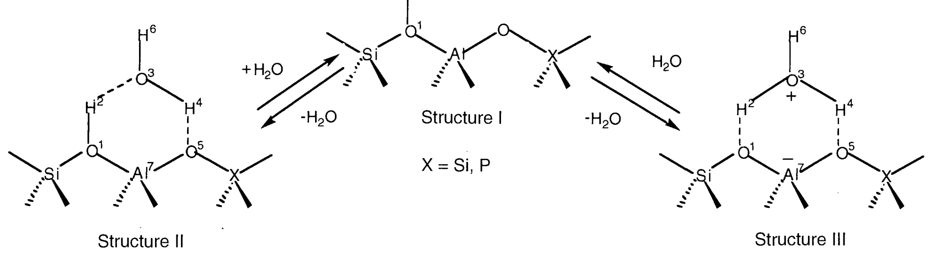

Scheme I

Here we show, by a combination of neutron diffraction and infrared (IR) spectroscopy, that H_3O^+ and hydrogen-bonded water coexist at the interior surface of a powerful new synthetic catalyst, HSAPO-34, which is structurally analogous to, but compositionally distinct from, the zeolitic mineral chabazite (*5*). Whereas in chabazite all the tetrahedral (T) sites are tenanted by either Si^{4+} or Al^{3+} ions, Al and P ions occupy the T sites alternately in HSAPO-34, and some Si ions reside in the sites normally occupied by P. HSAPO-34 is acknowledged to be a powerful catalyst, with good performance in converting methanol to light alkenes (*6*).

In HSAPO-34, there are two distinct kinds of bridging hydroxyls, characterized by IR stretching frequencies at 3625 cm^{-1} (the so-called high-frequency mode) and at 3600 cm^{-1} (the low-frequency mode) (Fig. 1). This finding is in agreement with recent neutron diffraction studies of dehydrated HSAPO-34, which revealed protons at four-ring and six-ring oxygen sites (*7*). Our earlier diffuse reflectance IR Fourier transform spectroscopy (DRIFTS) measurements (*3*), allied to quantitative microgravimetry on progressively dehydrated HSAPO-34, indicated that, at room temperature, there is a stoichiometric proton transfer from one of the Brønsted sites to bound water, thereby forming H_3O^+ (structure III). Our interpretation concurred with that of Jentys *et al.* (*8*) but it contradicted that of Parker *et al.* (*9*),

---

L. Smith, A. K. Cheetham, R. E. Morris, Materials Research Laboratory, University of California, Santa Barbara, CA 93106, USA.
L. Marchese, Dipartimento di Chimica I.F.M., Università degli Studi di Torino, 10125-Torino, Italy.
J. M. Thomas, P. A. Wright, J. Chen, Royal Institution of Great Britain, 21 Albemarle Street, London W1X 4BS, UK.

*To whom correspondence should be addressed.

who favored structure II, which is merely a hydrogen-bonded state. Theoretical studies by van Santen and Kramer (*10*), Pelmenschikov and van Santen (*11*), Sauer *et al.* (*12*), and Gale (*13*) all favor structure II in preference to III, although a very recent computation that used an ab initio local density functional procedure for a sizable cluster of T sites with bridging hydroxyls has shown that a molecule of methanol certainly, and a less basic molecule such as water possibly, may accommodate complete proton transfer from acid aluminosilicate catalysts (*14*).

Our most recent IR studies have revealed a hitherto undetected doublet at 765 and 795 cm^{-1} that could be assigned to "out-of-plane" γ modes of OH perturbed by H-bonds (Fig. 1). Overtones of these absorptions ($2\gamma_{OH...O}$) as well as overtones of "in-plane" δ modes ($2\delta_{OH...O}$) (the other deformation vibrations of Brønsted OH groups), also perturbed by H-bonds, can produce two Evans windows at 2700 and 1560 cm^{-1}. These observations compel us to reconsider our earlier assignment. It is now more likely that, as Pelmenschikov, van Santen, and co-workers (*2*) had earlier suggested, a loosely bound $H_2O...H^+$ complex (structure II) exists, because the spectral observations may also be rationalized as arising from Fermi resonance between the fundamental stretching and the overtone bending vibrations of such a complex.

Adsorption of water vapor onto HSAPO-34 (Fig. 2, curve a) depletes the IR absorption bands of the bridging OH (see negative peaks at 3625 and 3600 cm^{-1} in Figs. 1 and 2), whereas a new absorption appears at 3680 cm^{-1}, with a shoulder at 3650 cm^{-1}. When enough water vapor is added (sufficient to fill all the cavities of the HSAPO-34), the 3650 cm^{-1} shoulder becomes a dominant feature of the spectrum (Fig. 2, curve b), and simultaneously the deformation modes of the protons disappear; it is likely that in this case $H_5O_2^+$ dimers as well as clusters of hydrogen-bonded molecules akin to those in liquid water are formed (*15*). Such behavior indicates that two different bound water species coexist when the ratio of H_2O to H^+ is 1:1; that is, a protonated water (H_3O^+) and a hydrogen-bonded water.

Table 1. Fractional coordinates and U_{iso} (isotropic temperature factors) for hydrated HSAPO-34. The crystallographic space group is R-3 (hexagonal, no. 148) with lattice parameters a = 13.7706 (7) Å and c = 14.9840 (9) Å (numbers in parentheses are standard errors in the last digit or digits).

Atom	*x/a* (Å)	*y/a* (Å)	*z/c* (Å)	Occupancy	U_{iso} (Å^2)
P(1)	0.0040 (10)	0.2284 (9)	−0.3938 (6)	0.780	0.002
Si(1)	0.0040 (10)	0.2284 (9)	−0.3938 (6)	0.220	0.002
Al(1)	0.2303 (11)	0.2285 (11)	−0.3962 (8)	1.000	0.002
O(1)	0.9953 (9)	0.7327 (6)	0.4874 (5)	1.000	0.0125 (4)
O(2)	0.8801 (10)	0.7568 (5)	0.3690 (5)	1.000	0.0125 (4)
O(3)	0.8029 (4)	0.9056 (9)	0.3808 (4)	1.000	0.0125 (4)
O(4)	0.6752 (8)	0.9818 (6)	0.3292 (6)	1.000	0.0125 (4)
O(5)	0.775 (5)	0.118 (5)	−0.853 (4)	0.206 (7)	0.061 (8)
D(1)	0.327 (5)	0.168 (7)	−0.810 (3)	0.206 (7)	0.061 (8)
D(2)	0.820 (4)	0.124 (4)	−0.900 (3)	0.206 (7)	0.061 (8)
D(3)	1.350 (4)	0.386 (3)	−0.510 (3)	0.206 (7)	0.061 (8)
D(4)	0.899 (7)	0.775 (4)	0.310 (3)	0.171 (15)	0.061 (8)
O(6)	1.009 (7)	0.877 (7)	0.230 (5)	0.130 (9)	0.061 (8)
D(5)	0.918 (4)	0.011 (5)	−0.823 (4)	0.130 (9)	0.061 (8)
D(6)	0.792 (5)	−0.068 (4)	−0.785 (4)	0.130(9)	0.061 (8)

We have now conducted powder neutron diffraction studies (*16*) on deuterated well-crystallized specimens of hydrated HSAPO-34, the aim being to analyze the powder diffraction pattern by the Rietveld method. Here we report such a study, which provides direct evidence of the coexistence of the two types of bound water.

The powder sample was deuterated through exchange with D_2O at 60° to 80°C and was loaded with D_2O so that the amount of D_2O was equal to the number of D atoms present in the sample. Powder neutron diffraction data were collected at 10 K with a neutron wavelength of 1.5390 Å on the diffractometer at the National Institute of Standards and Technology (NIST). The structure was refined by the Rietveld method (*17*) with the GSAS suite of programs (*18*). The space group, R-3, and the preliminary positions of the framework atoms were taken from the structure of the dehydrated form of HSAPO-34 (*7*). Silicon atoms were placed exclusively at phosphorus sites and held at fixed fractional occupancies based on previous magic angle spinning nuclear magnetic resonance studies (*19*). The T–O bond distances in the framework were constrained early in the refinement to match known chemical trends, but these soft constraints were later removed. The positions of the O and D atoms from the water molecules and deuterons from the acid sites were subject to soft constraints with the use of an O–D bond distance of 1.00 Å. The fractional occupancies of the O and D atoms of the D_3O^+

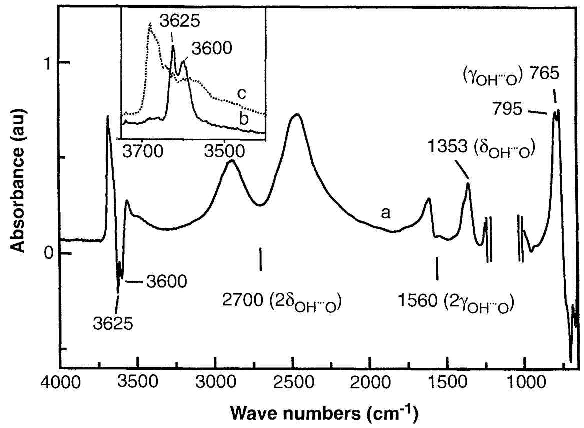

Fig. 1. Infrared spectra of H_2O adsorbed on HSAPO-34: Curve a was recorded once a dose of water sufficient to interact with all Brønsted OH was admitted (the spectrum is reported as a difference spectrum with respect to the dehydrated sample). Absorbance is in arbitrary units (au). **Inset**: Curve b is the spectrum in the OH stretching region of dehydrated HSAPO-34, and curve c is the spectrum obtained on the admission of H_2O (under the same conditions as curve a).

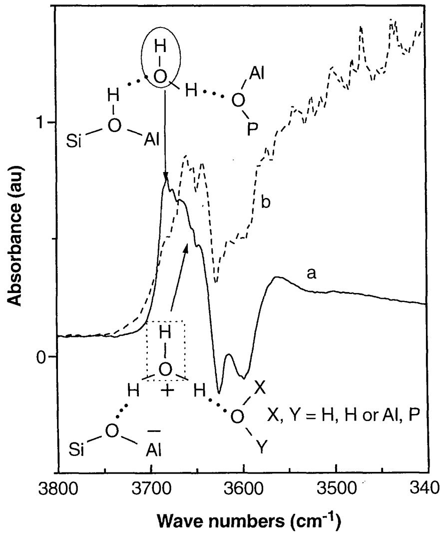

Fig. 2. Enlarged view of the OH stretching region of the IR spectra of H_2O adsorbed on HSAPO-34. Curve a is the same as in Fig. 1; curve b is the spectrum of the HSAPO-34 with H_2O filling the microcavities. Absorbance is in arbitrary units (au).

Table 2. Selected bond distances and angles for hydrated HSAPO-34. T(1) is either silicon or phosphorus.

Bond distances (Å)				Bond angles (degrees)	
		Framework atoms			
T(1)–O(1)	1.500 (10)	Al(1)–O(1)	1.812 (13)	T(1)–O(1)–Al(1)	143.6 (5)
T(1)–O(2)	1.551 (16)	Al(1)–O(2)	1.680 (19)	T(1)–O(2)–Al(1)	149.4 (5)
T(1)–O(3)	1.589 (15)	Al(1)–O(3)	1.682 (16)	T(1)–O(3)–Al(1)	150.4 (5)
T(1)–O(4)	1.587 (12)	Al(1)–O(4)	1.650 (14)	T(1)–O(4)–Al(1)	150.6 (5)
		*Hydronium ion**			
O(5)–D(1)	0.95	O(5)–O(1)	2.51	D(1)–O(5)–D(2)	99
O(5)–D(2)	0.91	D(3)–O(1)	1.50	D(1)–O(5)–D(3)	130
O(5)–D(3)	1.14	D(2)–O(2)	2.52	D(2)–O(5)–D(3)	127
				O(1)–D(3)–O(5)	144
		*Hydrogen-bonded water**			
O(6)–D(5)	0.99	D(4)–O(4)	2.37	D(5)–O(6)–D(6)	111
O(6)–D(6)	0.98	O(6)–O(2)	2.70	O(2)–D(4)–O(6)	146
O(6)–D(4)	1.89	O(6)–O(3)	2.50		
D(4)–O(2)	0.93	D(6)–O(3)	2.52		
D(4)–O(3)	2.58	D(6)–O(4)	2.66		

*No SDs are given because soft constraints were used.

and D_2O molecules were constrained to give the correct stoichiometries, and the isotropic temperature factors were constrained into groups representing T atoms, framework oxygens, and extra-framework species. Details of the refinement are given in Tables 1 and 2 and the final observed and calculated profiles are presented in Fig. 3.

Two acid sites were found in the refinement, D(3) and D(4). The fractional occupancies of these sites are: D(3), 20.6% in the vicinity of O(1); D(4), 17.1% attached to O(2). Water molecules are associated with each of these sites, designated by oxygen atoms O(5) and O(6), respectively. The water molecule close to the deuteron at O(2) has a low occupancy and is less well defined than the hydronium ion (Fig. 4). The deuteron from the acid site at O(2) is at a distance of 0.93 Å from the oxygen and 1.89 Å from the water molecule. The distances indicate that hydrogen bonding, rather than hydronium ion formation, is responsible for the interaction of a water molecule at this acid site. These deuterons are bent out the plane of the Si–O–Al bond by 34° and point toward the interior of the six-ring while lying slightly in the direction of the adjacent four-ring. This geometry would seem to be more perturbed than expected for an acid site deuteron and must result from the influence of some weak hydrogen bonding with the framework oxygen. One of the water molecule deuterons is at a distance of only 2.52 Å from the O(3) framework oxygen, which lies on the six-ring with O(2). The attraction of the deuterons on the water molecule toward these framework oxygens may also pull the acid site deuteron toward the four-ring, leaving it at a distance of 2.37 Å from O(4). The acid site deuteron is thus at a distance to form a weak hydrogen bond with the four-ring oxygen. These interactions may prevent the water molecule from further approaching the acid site and removing the deuteron from the framework.

A D_3O^+ ion is the predominant species, occupying 61% of the unit cells (Fig. 4). The acid deuteron sits 1.50 Å from the framework oxygen, O(1) and 1.14 Å from the oxygen of the D_3O^+ ion. The oxygen of the hydronium ion is located 2.51 Å from the acid site oxygen O(1). This position allows the H_3O^+ ion to sit in the large eight-ring channel of the structure. Another deuteron from the D_3O^+ ion interacts with the framework, if only weakly. The hydronium is rotated so that this deuteron lies 2.52 Å from framework oxygen O(2), at a distance that is short enough for a weak hydrogen bond to form. The interaction of the two deuterons with the framework causes the third deuteron on the D_3O^+ ion to point to the center of the eight-ring channel, where it is unable to interact with any of the framework oxygens.

In order to demonstrate the sensitivity of the data to our final model, we ran a series of calculations in which the two acid deuterons, D(3) and D(4), were placed in alternative positions. For the case in which they are both present as conventional Brønsted acid sites, hydrogen-bonded by water molecules, $\chi^2 = 1.478$; for two hydronium ions, $\chi^2 = 1.885$; and for the case in which D(3) is constrained to be bonded to O(1) and D(4) to O(6), $\chi^2 = 2.189$. For comparison, χ^2 for the final refinement was 1.199, showing that the data are very sensitive to the fine details of the model. Indeed, whereas our Fourier transform IR studies strongly imply coexisting structures II and III of Scheme I, our neutron powder diffraction studies provide excellent evidence of such coexistence.

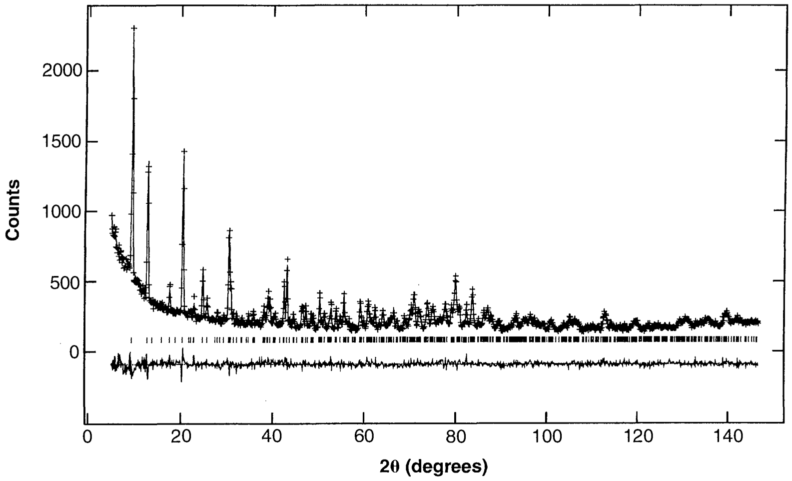

Fig. 3. Final observed, calculated, and difference profile plots for the neutron refinement of hydrated HSAPO-34. The data were collected at NIST with the use of neutrons of wavelength 1.5390 Å that were selected with a Cu(311) monochromator. The least-squares refinement converged to final agreement factors of $R_{wp} = 5.72\%$, $R_p = 4.63\%$, and $\chi^2 = 1.199$. The peak shape was fitted with a Gaussian function, with full width at half maximum parameters as follows: $U = 511$ (23), $V = -364$ (24), and $W = 210$ (6).

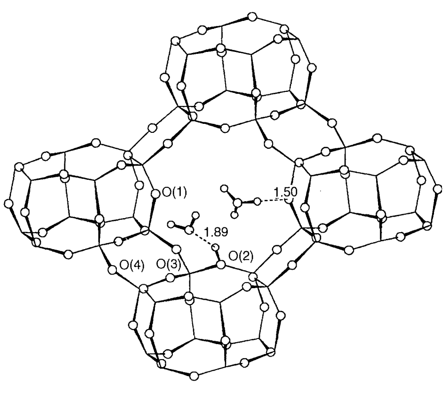

Fig. 4. A ball-and-stick representation of the structure of hydrated HSAPO-34, showing both the hydronium ion and a hydrogen-bonded water molecule. The figure depicts the oxygen and hydrogen atoms as spheres; the tetrahedral atoms (Al, P, and Si) are omitted.

Deeper insight into the nature of the proton transfer to water could doubtless be achieved if neutron scattering studies were made on progressively dehydrated (or hydrated) samples of HSAPO-34.

REFERENCES AND NOTES

1. J. Sauer, C. Kölmel, F. Haase, R. Ahlrichs, in *Proceedings of the Ninth International Zeolite Conference*, Montreal, Canada, 1992, T. van Ballmoos *et al.*, Eds. (Butterworth-Heinemann, Boston, MA, 1993), pp. 679–685.
2. A. G. Pelmenschikov, R. A. van Santen, J. Jänchen, E. C. Meijer, *J. Phys. Chem.* **97**, 11071 (1993).
3. L. Marchese, P. A. Wright, J. Chen, J. M. Thomas, *ibid.*, p. 8109.
4. M. F. M. Post, *Stud. Surf. Sci. Catal.* **58**, 392 (1991); J. M. Thomas, *Angew. Chem. Int. Ed. Engl.* **33**, 913 (1994); R. A. van Santen and G. J. Kramer, *J. Am. Chem. Soc.* **115**, 2887 (1993).
5. D. H. Olson and W. M. Meier, *Atlas of Zeolite Structures* (Butterworth-Heinemann, London, 1992), pp. 72–73.
6. J. A. Rabo, R. J. Pellet, P. K. Coughlin, E. S. Shamshon, in *Zeolites as Catalysts and Detergent Builders*, H. G. Karge and J. Weitkamp, Eds. (Elsevier, Amsterdam, 1989), pp. 1–40;Y. Xu, C. P. Grey, J. M. Thomas, A. K. Cheetham, *Catal. Lett.* **4**, 251 (1990).
7. L. Smith, L. Marchese, A. K. Cheetham, J. M. Thomas, P. A. Wright, unpublished data.
8. A. Jentys, G. Warecka, M. Derewnsky, J. A. Lercher, *J. Phys. Chem.* **93**, 4837 (1989).
9. L. M. Parker, D. M. Bibby, G. R. Burns, *Zeolites* **13**, 107 (1993).
10. R. A. van Santen and G. J. Kramer, *Chem. Rev.*, **95**, 637 (1995).
11. A. G. Pelmenschikov and R. A. van Santen, *J. Phys. Chem.* **97**, 10678 (1993).
12. J. Sauer, P. Ugliengo, E. Garroue, V. R. Saunders, *Chem. Rev.* **94**, 2095 (1994).
13. J. D. Gale, *Topics in Catalysis*, in press.
14. ______, unpublished data.
15. R. Buzzoni, S. Bordiga, G. Ricchiardi, G. Spoto, A. Zecchina, *J. Phys. Chem.* **99**, 11937 (1995).
16. A. K. Cheetham, J. M. Thomas, M. M. Eddy, D. A. Jefferson, *Nature* **299**, 24 (1982).
17. A. K. Cheetham and A. P. Wilkinson, *Angew. Chem. Int. Ed. Engl.* **32**, 1557 (1993).
18. A. C. Larson and R. B. Von Dreele, *Los Alamos Laboratory Rep. No. LA-UR-86-748* (1987).
19. B. Zibrowius, E. Loffler, M. Hunger, *Zeolites* **12**, 167 (1992).
20. Supported by the Materials Research Laboratory program of NSF under award no. DMR-9123048, by the Engineering and Physical Science Research Council (UK), and by an NSF Graduate Research Fellowship. We thank NIST for the access to their neutron diffraction facilities. J.C. and P.A.W. thank Unilever for financial support.

11 September 1995; accepted 10 November 1995

Mutagenesis in Mammalian Cells Induced by Triple Helix Formation and Transcription-Coupled Repair

Gan Wang, Michael M. Seidman, Peter M. Glazer*

When mammalian cells were treated with triplex-forming oligonucleotides of sufficient binding affinity, mutations were specifically induced in a simian virus 40 vector contained within the cells. Triplex-induced mutagenesis was not detected in xeroderma pigmentosum group A cells nor in Cockayne's syndrome group B cells, indicating a requirement for excision repair and for transcription-coupled repair, respectively, in the process. Triplex formation was also found to stimulate DNA repair synthesis in human cell extracts, in a pattern correlating with the inhibition of transcription in such extracts. These findings may have implications for therapeutic applications of triplex DNA and raise the possibility that naturally occurring triple helices are a source of genetic instability.

Triple helices can be formed when oligonucleotides bind in the major groove of duplex DNA at polypurine-polypyrimidine sequences (*1*). Triple helix formation has been used to block transcription initiation and elongation (*2*) and to cleave DNA in vitro (*3*). We have explored the use of triplex-forming oligonucleotides (TFOs) as a mechanism to deliver a tethered mutagen to a selected gene for the site-specific introduction of DNA damage and consequent mutations within cells (*4*, *5*). In the course of this investigation, we observed that TFOs have the potential to induce mutations in vivo even in the absence of a tethered mutagen.

Three oligonucleotides (AG10, AG20, and AG30) were designed to bind as third strands in the antiparallel triple helix motif (*1*) to part or all of a 30–base pair (bp) polypurine-polypyrimidine target site in the *supFG1* reporter gene within the simian virus 40 (SV40) vector, pSupFG1 (*5*, *6*). These oligonucleotides were tested for their ability to induce mutations in the vector within monkey COS cells (Table 1). The cells were first transfected with SV40 vector DNA (*7*). After 12 hours to allow chromatinization of the vector, the oligonucleotides were added to the growth medium at a concentration of 2 μM (*8*). Two days later, the vector DNA was harvested from the cells for analysis of *supFG1* gene mutations (*9*). Oligonucleotide AG30 generated mutations in the target gene at a frequency of 0.27%, 13 times above the spontaneous background in the assay. In contrast, AG10 and AG20, which show weaker third-strand binding to *supFG1*, were less effective in producing mutations. As an additional control, an oligonucleotide of 30 nucleotides consisting of a mixture of all four bases (Mix30) (*5*, *6*) was also tested. This oligonucleotide did not form a detectable triple helix with *supFG1* (*5*) and it did not generate any mutagenesis above the background. The *supFG1* mutations generated

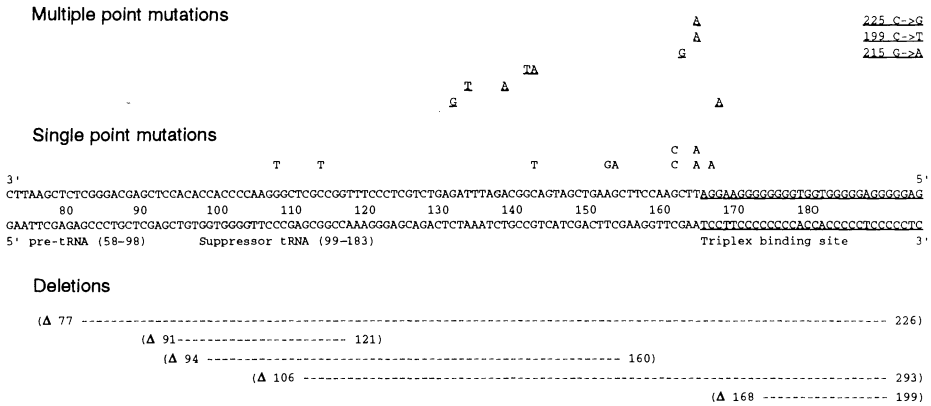

Fig. 1. Sequences of *supFG1* mutations induced by triple helix formation in COS cells. Three classes of mutations were observed, including single point mutations, deletions, and multiple, simultaneous point mutations, as indicated. The base substitutions listed above the corresponding *supFG1* gene sequence represent changes with respect to the upper strand. The multiple point mutations are underlined, with each set of simultaneous changes presented on a separate line. Point mutations occurring outside of the listed sequence are indicated by position numbers, with the involved base changes given. The deletions are presented below the gene sequence, with the deletion end points indicated. The triplex target site at base pairs 167 to 196 of the *supFG1* gene is indicated.

G. Wang and P. M. Glazer, Department of Therapeutic Radiology, Yale University School of Medicine, P.O. Box 208040, New Haven, CT 06520–8040, USA.
M. M. Seidman, OncorPharm, 200 Perry Parkway, Gaithersburg, MD 20877, USA.

*To whom correspondence should be addressed.